



# Mapping burn severity and monitoring CO content in Türkiye's 2021 Wildfires, using Sentinel-2 and Sentinel-5P satellite data on the GEE platform

Osman Salih Yilmaz<sup>1</sup> · Ugur Acar<sup>2</sup> · Fusun Balik Sanli<sup>2</sup> · Fatih Gulgen<sup>2</sup> · Ali Murat Ates<sup>3</sup>

Received: 24 November 2022 / Accepted: 1 January 2023 / Published online: 10 January 2023  
© The Author(s), under exclusive licence to Springer-Verlag GmbH Germany, part of Springer Nature 2023

## Abstract

This study investigated forest fires in the Mediterranean of Türkiye between July 28, 2021, and August 11, 2021. Burn severity maps were produced with the difference normalised burned ratio index (dNBR) and difference normalised difference vegetation index (dNDVI) using Sentinel-2 images on the Google Earth Engine (GEE) cloud platform. The burned areas were estimated based on the determined burning severity degrees. Vegetation density losses in burned areas were analysed using the normalised difference vegetation index (NDVI) time series. At the same time, the post-fire Carbon Monoxide (CO) column number densities were determined using the Sentinel-5P satellite data. According to the burn severity maps obtained with dNBR, the sum of high and moderate severity areas constitutes 34.64%, 20.57%, 46.43%, 51.50% and 18.88% of the entire area in Manavgat, Gündoğmuş, Marmaris, Bodrum and Köyceğiz districts, respectively. Likewise, according to the burn severity maps obtained with dNDVI, the sum of the areas of very high severity and high severity constitutes 41.17%, 30.16%, 30.50%, 42.35%, and 10.40% of the entire region, respectively. In post-fire NDVI time series analyses, sharp decreases were observed in NDVI values from 0.8 to 0.1 in all burned areas. While the Tropospheric CO column number density was 0.03 mol/m<sup>2</sup> in all regions burned before the fire, it was observed that this value increased to 0.14 mol/m<sup>2</sup> after the fire. Moreover, when the area was examined more broadly with Sentinel 5P data, it was observed that the amount of CO increased up to a maximum value of 0.333 mol/m<sup>2</sup>. The results of this study present significant information in terms of determining the severity of forest fires in the Mediterranean region in 2021 and the determination of the CO column number density after the fire. In addition, monitoring polluting gases with RS techniques after forest fires is essential in understanding the extent of the damage they can cause to the environment.

**Keywords** dNBR · dNDVI · Forest fire · Google Earth Engine · Carbon Monoxide · TROPOMI

## Introduction

Forests are renewable natural resources that contribute significantly to the economy of countries and play a decisive role in the climate and ecosystem (Dixon et al. 2022). The

temperature and low humidity are two important factors that cause forest fires (Masinda et al. 2022). In addition, the increase in wind effect causes further damage to forest areas during a fire (Esemem 2011; Efthimiou et al. 2020). Detection of the damaged regions after a fire is critical in revealing the severity of the fire and its ecological effects on the ecosystem (Kulakowski and Veblen 2007; Li et al. 2018). Burn severity maps reflecting changes in vegetation and forest soil

Communicated by H. Babaie.

✉ Osman Salih Yilmaz  
osmansalih.yilmaz@cbu.edu.tr

Ugur Acar  
uacar@yildiz.edu.tr

Fusun Balik Sanli  
fbalik@yildiz.edu.tr

Fatih Gulgen  
fgulgen@yildiz.edu.tr

Ali Murat Ates  
murat.ates@cbu.edu.tr

<sup>1</sup> Demirci Vocational School, Manisa Celal Bayar University, 45900 Manisa, Türkiye

<sup>2</sup> Geomatic Engineering Department, Yildiz Technical University, 34220 Istanbul, Türkiye

<sup>3</sup> Computer and Instructional Technologies Department, Faculty of Education, Manisa Celal Bayar University 45900, Manisa, Türkiye

characteristics have a high priority in determining short-term measures to be taken after a fire (García-Llamas et al. 2019). Forest fire severity is measured by collecting data on tree mortality, canopy loss, or bole and crown scorch (Keeley 2008). However, fieldwork after a fire in steep and inaccessible forest areas is quite challenging. Today, in parallel with the developments in satellite technologies, remote sensing (RS) systems have started to be used to determine forest burn severity. RS utilises optical sensors that can detect data from large areas difficult to reach in forest fires, beyond the visible region of the electromagnetic spectrum, and provide continuous data. Decreases in chlorophyll, especially in burning regions, cause an increase in the reflection of the visible region of the electromagnetic spectrum while a decrease in the near-infrared region (Escuin et al. 2008). These critical changes in the electromagnetic spectrum make it possible to detect burning areas with RS (García-Llamas et al. 2019). Satellite images before and after the fire in large forest areas give information about the severity of the fire and its effects on the region (Hantson et al. 2013; Teodoro and Amaral 2019).

Burnt areas are most mapped using medium-resolution, multispectral satellite images (Goodwin and Collett 2014). The electromagnetic spectrum's near-infrared (NIR) and short-wave infrared (SWIR) ranges (0.7 to 2.4  $\mu\text{m}$ ) are sensitive to post-fire charred vegetation and various substances. Medium and low-resolution satellite images with this band range, such as 30 m spatial resolution Landsat, 250 m spatial resolution Medium Resolution Imaging Spectroradiometer (MODIS), 1 km spatial resolution Advanced Very High-Resolution Radiometer (AVHRR), are used for this purpose (Storey et al. 2021). Very High Resolution (VHR) satellite images are also helpful for disaster management and damage assessment (Chung and Kim 2021). Higher spatial resolution images can better understand the ecological impacts of burning areas (Eva and Lambin 2000). For this purpose, Landsat images that provide 30 m spatial and 16 days temporal resolution, and Sentinel-2 A/B satellite constellation, which provides 10 m spatial and five days temporal resolution, offer advantages in terms of damage detection and fire monitoring immediately after the fire event.

Indices determined using mathematical operations of spectral bands are used to determine the plant phenology cycle pre-and post-fire and produce burn severity maps. Commonly, differenced normalised burn ratio (dNBR) and the differenced normalised difference vegetation index (dNDVI) are used to measure the impact of fire on biomass (Key and Benson 2006; Mathews and Kinoshita 2021). In general, both indices successfully detect biomass loss relative to the pre-fire state of an ecosystem. While dNBR is defined as the differences in NBR index before and after the fire, dNDVI is the NDVI differences before and after the fire (van Gerrevink and Veraverbeke 2021). The normalised burn rate (NBR) is used to observe spectral changes after a fire event (Lentile et al.

2006; Gibson et al. 2020). NDVI is the most basic index to show vegetation presence and health. At the same time, the normalised difference vegetation index (NDVI) time series can explain the increases and decreases in photosynthetic activity, vegetation, and biomass (Cheret and Denux 2011). Besides RS techniques, the composite burn index (CBI) field protocol and modified CBI method (GeoCBI), widely used in field studies, are defined as the measurement average of more than one environmental variable of post-fire conditions (Key and Benson 2006; Picotte et al. 2021).

Several studies have been carried out to detect fire areas with RS techniques. Quintano et al. (2011) mapped the burning areas with Gaussian functions, kernel-based smoothing, and adaptive thresholding algorithms on MODIS satellite images. They used the burn area index (BAI) and NBR to detect burned areas. They tested the accuracy of the maps with situ Global Positioning System (GPS) measurements. For this purpose, they used  $j$  statistics and obtained a high accuracy of ( $j > 0.8$ ). Parks et al. (2014) proposed a new Landsat-based burn severity metric, the relativised burn ratio (RBR), which provides an alternative to dNBR and RdNBR. According to the results in 18 fire zones, dNBR ( $R^2 = 0.761$ ), RdNBR ( $R^2 = 0.766$ ) and RBR ( $R^2 = 0.786$ ) were found. Botella-Martínez and Fernández-Manso (2017) calculated the dNBR, RdNBR and RBR indices for nine fire zones in the Valencia region based on Landsat 8 images. Unburned in each index is divided into low, moderate, and high classes. In the study, the degree of relationship between pre-fire vegetation and burn severity was examined by analysis of variance. Youn & Jeong (2019) used dNBR to map the severity of burning areas in Sokcho forests in South Korea using Sentinel-2 images. Gibson et al. (2020) tested the performance of traditional burn indices with the random forest (RF) algorithm using Sentinel-2 images. Atun et al. (2020) examined forest fires in Athens, Greece, with NBR, dNBR, RBR and NDVI. In their study, the size of the vegetation destroyed by the fire and the probability of exposure to forest fire were determined. Delcourt et al. (2021) used Sentinel-2 images to test the use of the most common spectral index in determining burn severity and found that the dNBR index correlated reasonably well with field data. Hu et al. (2021) aimed to explain the capacity of deep learning (DL) models to map burned areas from single-time multispectral images automatically. For this purpose, several semantic segmentation network architectures and machine learning (ML) algorithms such as U-Net, HRNet, Fast-SCNN and DeepLabv3+ were tested using Sentinel-2 and Landsat-8 images at three wild-fire sites. Giddey et al. (2022) conducted field observations to confirm the dNBR index on Sentinel-2 images in the Afrotropical forest of South Africa. They found a strong correlation between field observations and dNBR ( $R^2 = 0.69$ ). There are studies on vegetation change, especially after the fire in the burned areas. Cheret & Denux (2011) evaluated the

fire susceptibility of Mediterranean vegetation by analysing the NDVI time series of MODIS Terra images from 2000 to 2006. Lanorte et al. (2014) used SPOT-VEGETATION NDVI time series and Fisher-Shannon (FS) statistical method to investigate the vegetation dynamics before and after the fire. Uyeda et al., (2015) used MODIS NDVI time series to monitor post-fire recovery in chaparral thickets in Southern California. (Bar et al. 2020) compared the performance of three machine-learning approaches for burnt area detection based on Sentinel-2 and Landsat-8 data in the GEE framework. Their results show superior classification accuracy of 97–100% for the Classification and Regression Tree (CART) and RF algorithms while slightly lower accuracy for the Support Vector Machine (SVM). Seydi et al. (2021) (Seydi et al. 2021) detected forest fires in Australia and burned areas using the k-Nearest Neighbors (kNN), RF, and SVM machine learning algorithms using Sentinel-2 and MODIS images on the GEE platform. MODIS images (MCD12Q1) were used to detect LULC in the study. They determined that the RF algorithm was more successful than the others in detection of the burned areas. Smith-Ramírez et al. (2022) investigated the short- and long-term behaviour of the Chilean sclerophyllous vegetation between 1985 and 2015 with Landsat images.

Burning is a chemical event that occurs with the oxidation and decomposition of organic matter and living and dead vegetation (De la Rosa et al. 2008). As a result of this chemical event, various polluting gases are emitted into the environment. Different gases such as carbon dioxide (CO<sub>2</sub>), methane (CH<sub>4</sub>), and carbon monoxide (CO) can be listed as examples of these polluting gases (Satyendra et al. 2013). During a forest fire, these gases and other pollutants penetrate the air in large quantities (Michel et al. 2005). Reahard et al., (2010) calculated various pollutant gases from sugarcane and swamp burning off the coast of Louisiana, USA, using MODIS, Advanced Spaceborne Thermal Emission and Reflection Radiometer (ASTER), and Landsat-TM images. The TROPospheric Monitoring Instrument (TROPOMI) sensor on the Sentinel-5P satellite helps to monitor the gases emitted after a fire and make environmental assessments (Xulu et al. 2021). Schneising et al. (2019) developed a new algorithm, Weighting Function Modified Differential Optical Absorption Spectroscopy (WFM- DOAS), to obtain CO and CH<sub>4</sub> values simultaneously from the Sentinel-5P satellite data. This algorithm was developed to perform mutual validation with other algorithms. Vahid et al. (2020) carried out Spatio-temporal changes in the amount of CO in the air in Iran for 14 months through Sentinel-5 data. Magro et al. (2021) evaluated the spatial distribution of CO and CH<sub>4</sub> after the fire in Portugal with Sentinel 5P images. CO concentrations were observed on 21 July 2019 and 7 August 2018, with CO columns exceeding  $4.5 \times 10^{18}$  and  $6 \times 10^{18}$  molecules/cm<sup>2</sup>, respectively.

Many studies have been conducted using Sentinel-5P satellite data for air pollution monitoring, especially during the COVID-19 pandemic period. For example, Mehmood et al. (2021) monitored column number density values of NO<sub>2</sub> and PM<sub>2.5</sub> pollutants in three provinces of Pakistan from March 22, 2020 to June 30, 2020 (during COVID-19). Sentinel-5P TROPOMI data for NO<sub>2</sub> value and PM<sub>2.5</sub> value were recorded from sampling sites. Faisal et al. (2021) monitored CO, O<sub>3</sub>, SO<sub>2</sub>, and NO<sub>2</sub> polluting gases with Sentinel-5P images during the COVID-19 pandemic (from November 2020 to December 2020) in Indonesia. In this study, the decrease in CO, NO<sub>2</sub>, and O<sub>3</sub> gas column number density was determined. Ghasempour et al. (2021) calculated NO<sub>2</sub> and SO<sub>2</sub> gas column number density values using Sentinel-5P TROPOMI, and Aerosol Optical Depth (AOD) from MODIS data in Türkiye during the COVID-19 period in the GEE platform. Shami et al. (2022) monitored NO<sub>2</sub> and CO gas column number density during the COVID-19 lockdown period in Iran as well. They used Sentinel-5P TROPOMI data on the GEE platform in three periods covering the dates 11 March–8 April 2019, 2020 and 2021 in the study.

This study was examined under two primary motivations. In the first section, the significant wildfire that emerged at five different points on the southern coast of Türkiye that affected the Mediterranean coastline for about 15 days was examined with dNBR and dNDVI indexes on the GEE platform using Sentinel-2 satellite images. In the second section, it is evaluated that burn severity influences CO column number density. The changes in CO gas emitted into the atmosphere during the wildfire were monitored using TROPOMI data based on Sentinel-5P satellite observations. Thus, the spread of polluting gases, which are difficult to follow during a forest fire, was observed, and the effects of the fire on environmental pollution were analysed. In addition, Sentinel-5P satellite images are an instrumental dataset in monitoring polluting gases emitted during a fire. This study showed that using Sentinel-2 and Sentinel-5P data would be significant in monitoring forest fires and revealing wildfire's atmospheric effect. There are many studies on the use of indexes whose accuracy has been proven by many studies in the examination of forest fires. In addition, there are studies investigating atmospheric pollution using Sentinel 5P satellite data. However, much more work is still needed on this topic. Examining the forest fires, which caused great destruction in 2021, together with their polluting effects on the environment, reveals the innovative aspect of this study. This study is essential in two aspects; it provides a basis for monitoring vegetation recovery in the forest after a fire, and the other important aspect is that it is a guide for the use of satellite-based data in future forest fires for rapid damage detection, monitoring the spread of polluting gases, and taking the necessary precautions.

## Study area

This study examines the large wildfires that began on 28.07.2021 and lasted about 15 days along the Mediterranean coast of Türkiye. The wildfire broke out at five different points within the borders of the Manavgat and Gundogmuş districts of Antalya and Marmaris, Bodrum, and Koycegiz districts of Mugla (Fig. 1).

Antalya province is located on the western Mediterranean coast of southwest Türkiye. In general, the summers are hot and dry in that region. The maquis is the dominant vegetation in the Mediterranean region. There are red pine forests in the upper parts of the city (<https://www.antalya.bel.tr/>). The highest temperature was at 45°C between 1930 and 2020 in Antalya, while the lowest was at -4.6°C (<https://www.mgm.gov.tr/>). Manavgat district is about 77 km away from the city centre of Antalya. It is the second-largest district in terms of surface area and the third-largest district in terms of population in Antalya (<https://www.tuik.gov.tr/>). The Taurus Mountains surround the Manavgat to the north. The district has a rough terrain besides flat plains from the sea to the interior. The Alara Stream and Karpuz Stream, which form the eastern borders, and the Manavgat River from the district centre and the Manavgat Waterfall are world-famous in Türkiye. It is the town of Gundogmus, approximately 149 km from the centre of Antalya. It is a town built on the Western Taurus and Geyik Mountains.

The average altitude from the sea is 900 m. Although the Mediterranean climate is dominant, it shows somewhat continental climate characteristics in winter. Mugla, located in the South of Türkiye, is in the Aegean region, although a small part of it lies in the Mediterranean. Mugla is under the influence of the Mediterranean climate. The mountains extend parallel to the sea and reach 800 m. Mugla is one of the wealthiest regions of Türkiye in terms of forests. Mugla's highest temperature was measured at 42.1 °C between 1928–2020, while the lowest was -12.6 °C (<https://www.mgm.gov.tr/>). Marmaris, surrounded by Datca Peninsula and Kerme Bay in the west, Ula in the north, Balan Mountain, Karadag and Daily Hills in the east, and the Mediterranean Sea in the South, is one of the most important districts of Mugla. It is approximately 55 km from Mugla city centre. In the district, where the Mediterranean climate is dominant, summers are hot and dry, while winters are warm and rainy. Bodrum, one of the most important touristic places in the region, is located 110 km from the centre of Mugla, and most of the territory of Bodrum is in a peninsula that bears its name. It has a climate consisting of the synthesis of Aegean and Mediterranean climates. The historically significant town of Koycegiz, located approximately 73 km from the centre of Mugla, took its name from the Koycegiz Lake, which has a coast. The Mediterranean climate is dominant in the coastal parts of the region, and in the mountainous parts, the continental climate is prevalent.

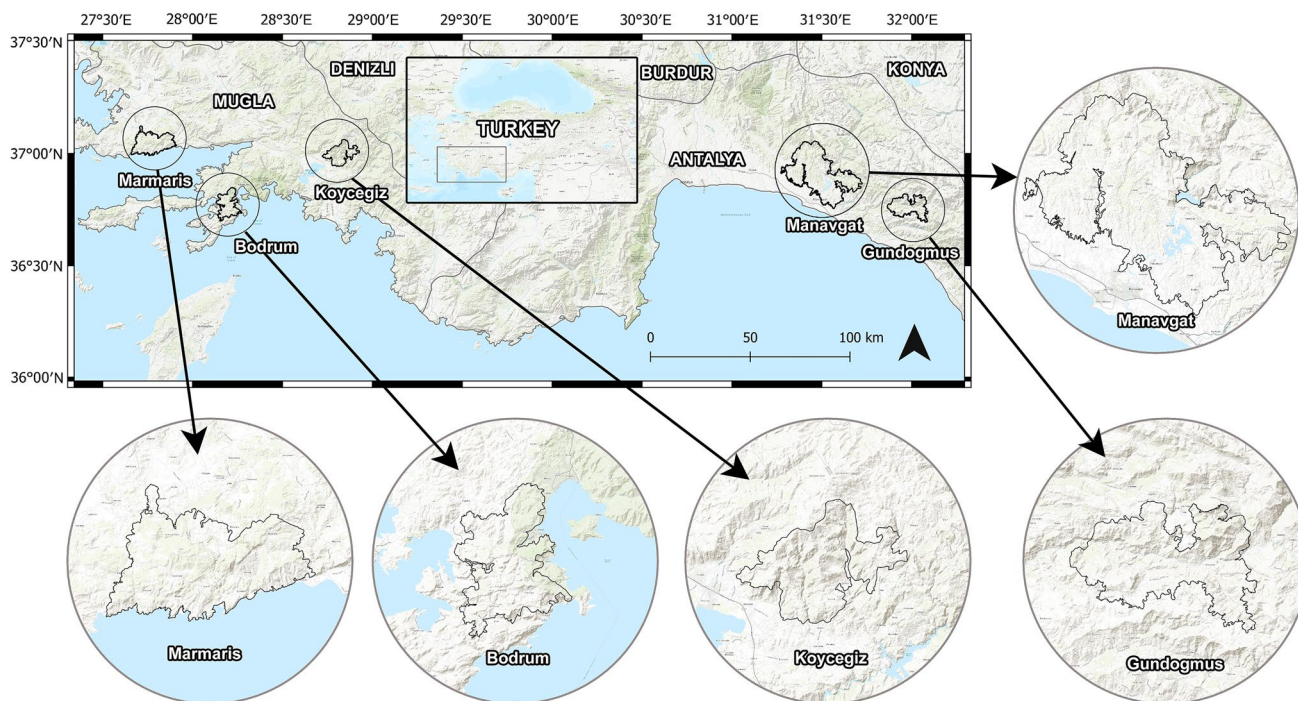


Fig. 1 Study area

## Material and method

### Satellite data

In the first step of the study, Sentinel-2 (MSI) images that the GEE platform provides free access to were used. For this purpose, image collections were created before and after the fire, considering each region's fire exit and end times. The image collection date ranges for each fire zone are given in Table 1. Sentinel-2 satellite, a part of the European Commission's (EC) Copernicus program, consists of two satellites sent by European Space Agency (ESA), Sentinel-2A and Sentinel-2B. The Multispectral Instrument (MSI) sensor used in Sentinel-2A and Sentinel-2B satellites has a 12-bit radiometric resolution (Astola et al. 2019). Each one has 13 spectral bands, and the spatial resolution of the band ranges from 10 to 60 m. In this study, "COPERNICUS/S2\_SR" (L2A) images in GEE are Bottom of Atmosphere (BOA) corrected images in World Geodetic System 1984 (WGS 1984) coordinates (Cordeiro et al. 2021). After applying the water and cloud masks to the created image collections, the mosaicking was done and turned into a single image with median statistics. Keeping the pre-fire date range wider or smaller did not significantly affect the pre-burn spectral reflectance. However, the date range is essential in choosing the dates after the fire in terms of the sharp change in the pixel reflection values in the entire burned area.  $NBR_{pre}$ ,  $NBR_{post}$ ,  $dNBR$ ,  $NDVI_{pre}$ ,  $NDVI_{post}$ , and  $dNDVI$  indexes were calculated on the images with the median statistics applied with JavaScript code on the GEE platform. In addition to these indices, an image collection was created to include the months of May and September of 2021. Time series analysis was performed by calculating NDVI for each collection created.

In the second stage of the study, environmental pollution was investigated by producing maps of CO, which is the pollutant gas emitted by burning forests in the Mediterranean Region. For this purpose, Sentinel-5P satellite images were used. The TROPOMI sensor integrated with the satellite is a Top of Atmosphere (TOA) nadir imaging spectrometer covering wavelength bands between ultraviolet and short-wave infrared. TROPOMI operates in a push-broom

configuration with a swath of ~2600 km on the Earth's surface (Tian et al. 2022). The TROPOMI instrument measures the column number density of polluting gases such as CH<sub>4</sub>, Sulfur dioxide (SO<sub>2</sub>), Nitrogen dioxide (NO<sub>2</sub>), Ozone (O<sub>3</sub>), CO and atmospheric formaldehyde (HCHO) (Faisal et al. 2021). TROPOMI observes the global amount of CO using clear sky and cloudy sky Earth illumination measurements in the 2.3 μm spectral range of the SWIR portion of the electromagnetic spectrum. TROPOMI precise sky observations provide CO accumulation columns sensitive to the tropospheric boundary layer (Magro et al. 2021). For cloudy environments, column sensitivity varies with light path. There are two versions of Sentinel-5P datasets, Near Real-Time (NRTI) and Offline (OFFL). The NRTI product is given in 5-min data granules, while the OFFL data is given according to each satellite orbit (Verhoelst et al. 2021). Processing algorithms are the same for both products. For both OFFL and NRTI products, the quality value  $qa\_value > 0.5$  is required when using CO data (Tian et al. 2022). TROPOMI CO data consists of 1,000 m thick vertical layers equidistant from the ground for each pixel. Sentinel-5P images are represented on the GEE platform with a spatial resolution of 0.01 arc degrees (1.11 km) (Ghasempour et al. 2021). In this study, in which Sentinel-5P TROPOMI NRTI product was used, images were obtained at intervals of 2–3 days, covering the fire areas completely, considering the dates in Table 1, in order to understand the spread of CO gas.

### Wind data

MERRA-2 is a model created by the National Aeronautics and Space Administration (NASA) Office of Global Modelling and Assimilation (GMAO) using the GEOS-5.12.4 system (Reichle et al. 2017a). Since 1980, MERRA-2 has provided hourly global forecasts of atmospheric conditions (Reichle et al. 2017b), using hourly wind speed and direction at a grid-level (m/s)  $0.5^\circ \times 0.625^\circ$  between July 7, 2021 and August 22, 2021 for each fire zone.

### Türkiye air quality monitoring network

The Türkiye Air Quality Monitoring Network is affiliated with the Turkish Ministry of Environment and Urbanization, which records the concentration of pollutants every hour and has 355 monitoring stations. Other stations in the fire zones do not measure CO gas. Therefore, in this study, the CO measurement data of Serik station, which is 34 km away from the Manavgat district, and covers a large area, was used. The data collected from satellite observations over an average of two days, covering pre-fire and post-fire, were compared with the station measurements. The data used were downloaded from the (<https://www.havaizleme.gov>).

**Table 1** Satellite image date ranges used for the collection

Region	Pre-fire start/end	Post-fire start/end
Manavgat	01-07-2021/25-07-2021	26-07-2021/08-08-2021
Gundogmus	01-07-2021/25-07-2021	26-07-2021/08-08-2021
Marmaris	01-07-2021/25-07-2021	26-07-2021/04-08-2021
Bodrum	01-07-2021/25-07-2021	26-07-2021/08-08-2021
Koycegiz	01-07-2021/25-07-2021	02-08-2021/19-08-2021

tr/) platform. In this study, the TROPOMI data accuracy was evaluated using ground measurement stations.

## Methodology

Fire partially destroys the land surface by reducing vegetation, density, greenery, and water content. This change alters the spectral response of the land surface (Boer et al. 2008). The detected spectrum's visible and NIR reflectivity decreases, and the SWIR reflectivity increases (Lentile et al. 2006). NBR is an effective method to measure burn severity in various plant species. This index can determine the severity of burns by determining chemical changes such as blackening and powdery mildew caused by burning in vegetation. Green plants reflect the NIR wavelength highly and give a high reflection in the SWIR band in dry and unburned soil, and the NBR index was calculated using these features (Mathews and Kinoshita 2021). The NBR index is the ratio of the reflectance difference between the two spectra, expressed as Eq. 1 (Key and Benson 2006). The NBR index takes values ranging from -1 to +1.

$$NBR = \frac{NIR - SWIR}{NIR + SWIR} \quad (1)$$

where the NIR band for Sentinel-2 images is B8, and the SWIR band represents B12. The B8 has a 10 m spatial resolution, while the B12 has 20 m. In this study, B12 was resampled to a spatial resolution of 10 m by the bilinear interpolation method. Thus, the resulting maps have a 10 m spatial resolution.

Although the NBR index is used to show the area affected by the fire on a single map, the dNBR calculated with the NBR index differences calculated before and after the fire is widely used to measure the severity of the fire. dNBR index is calculated by Eq. 2. Areas with high dNBR indicate the degree of severe burn, while low and negative values represent less burn severity and unburned areas.

$$dNBR = NBR_{pre} - NBR_{post} \quad (2)$$

Key & Benson (2006) suggested burn severity levels were used in this study. As shown in Table 2, burn severity levels were checked at five different levels.

The NDVI can predict vegetation and biomass change pre-fire and post-fire (Mathews and Kinoshita 2021). The NDVI was developed by Rouse et al. in 1974. It uses red and NIR reflected by vegetation. Healthy vegetation absorbs most of the visible light and reflects most NIR. In contrast, unhealthy or sparse vegetation reflects the most visible and very little NIR (Rouse et al. 1974). NDVI calculations for a given pixel always result in a value ranging from (-1) to (+1) (Arehki et al. 2019). Very low NDVI values (<0.1) indicate barren rock, sand and barren areas. Soil gets a shallow NDVI

**Table 2** Burn severity (dNBR) classification (not scaled)

Severity Level	dNBR Values
High	> 0.66
Moderate-High	0.44–0.65
Moderate-Low	0.27–0.43
Low	0.1–0.26
Unburned	< 0.1

**Table 3** Burn severity (dNDVI) classification

Severity Level	dNDVI Values
Very High	> 0.45
High	0.33–0.44
Moderate	0.20–0.33
Low	0.13–0.20
Very Low	0.08–0.13
Unburned	< 0.07

value, and this value is between 0.1–0.2. Shrub, pasture and sparse vegetation areas take values between 0.2–0.5. High NDVI values represent dense green areas such as forests and cultivated areas (Dindaroglu et al. 2021).

NDVI (Eq. 3) was calculated for Sentinel-2 images in the study. The vegetation index was used to estimate biomass change before and after the fire. Thus, spatial and ecological changes in the distribution of vegetation after the fire can be determined (Hope et al. 2007; Mathews and Kinoshita 2021). Also shown is Eq. 4 the dNDVI obtained using the pre-fire and post-fire differences.

$$NDVI = \frac{NIR - RED}{NIR + RED} \quad (3)$$

$$dNDVI = NDVI_{pre} - NDVI_{post} \quad (4)$$

where The RED band represents B4. Both bands have a spatial resolution of 10 m.

(Morante-Carballo et al. 2022) divided the dNDVI index into six classes to determine burn severity (Table 3). In this study, the dNDVI index was calculated with the NDVI differences calculated pre- and post-fire and reclassified into six classes.

## Accuracy Assessment

The accuracy assessment of the study was examined using a confusion matrix. The confusion matrix was constructed with four parameters: true positive (TP), false positive (FP), true negative (TF), and false negative (FN) (Table 4). Various accuracy values can be calculated using this matrix. As shown in Table 5 for this study: overall accuracy (OA), kappa ( $\kappa$ ), recall, specificity, precision (PCC), balanced accuracy (BA), F1-score (FS), false alarm (FA), miss-detection (MD) were calculated (Wang et al. 2018; Seydi et al. 2021).

**Table 4** Confusion matrix (Wang et al. 2018; Seydi et al. 2021)

		Predicted	
		Burned	Unburned
Actual	Burned	TP	FN
	Unburned	FP	TN

This work was carried out in JavaScript using the GEE platform. The work consists of the following steps. (1) First, appropriate satellite passes were detected at the fire date (2) Water masks were applied to the cloud and selected images. (3) Created collections were resampled, mosaics created, and median statistics applied. (4) NBR and NDVI index were calculated for pre-fire and post-fire images. (5) dNBR and dNDVI were calculated using NBR and NDVI pre- and post-fire index results. (6) Burn severity maps, and combustion areas were created according to the calculated dNBR and dNDVI. (7) NDVI time series analyses were performed for the burned areas. (8) The correlation between dNDVI and dNBR after the fire was determined. (9) Created "ImageCollection" for CO concentration for pre-fire, fire time and post-fire dates. (10) qa\_value > 0.5 masks were applied. (11) Mosaics were created, and median statistics were applied. (12) The correlation between the CO concentration detected by the TROPOMI sensor and the values measured with the Serik station of the Turkish Air Quality Monitoring Network was calculated. The methodology flow-chart is given in Fig. 2.

## Results

### Burned area mapping

The accuracy assessments obtained by constructing the confusion matrix of both burn severity maps are given in Tables 6 and 7. The accuracy assessment for each of the

five fire zones was calculated separately. The study's accuracy was evaluated with random points ranging from 249 to 1738 according to the size of the burned area. The accuracy assessment was above 80%, revealing that the fire areas are generally correctly detected. Although the OA value in the dNDVI was generally successful compared to the dNBR, it was seen that the dNBR was more successful in other validation metrics. In the Manavgat forest fire, while OA was 85.06% in the dNDVI, it was 81.98% in the dNBR. The specificity calculated in the dNBR was 63.15%, and the PCC value was 87.01%. At the same time, the FA value was calculated as 37.99 and the MD as 0. When these values are evaluated, it can be said that the dNBR gives more accurate results than the dNDVI. In Gundogmus, another fire zone, the OA value was calculated as 80% in the dNBR, while the OA value was calculated as 74.79% in the dNDVI. It was seen that the dNBR was more successful in other accuracy metrics. When the forest fire in Marmaris was examined, while the OA value was 89.28% in the dNBR, the OA value was 93.66% in the dNDVI. When the other metrics in this region were examined, the dNDVI gave a more successful result than the dNBR. In Bodrum and Koycegiz fires, the OA values of both indexes were quite close to each other. When other metrics are examined, it can be said that dNBR is more successful in the Bodrum fire and dNDVI is more successful in the Koycegiz fire.

The maps produced with the dNBR and dNDVI indices used to map the forest fires in the study area are given in Fig. 3. For the dNBR, there are five levels of burn severity: high, medium-high, medium-low, low, and unburned (Key and Benson 2006). The dNDVI is divided into six different classes: unburned, very low severity, low severity, moderate severity, high severity, and very high severity (Morante-Carballo et al. 2022).

The burn severity regions calculated according to the dNBR and dNDVI indexes are given in Table 8. When the burned areas found with the dNBR were examined, the total burned area in the Manavgat district of Antalya

**Table 5** The metrics which were used in the accuracy assessment of burn severity maps (Wang et al. 2018; Seydi et al. 2021)

OA	$\frac{(TN+TP)}{N}$
$\kappa$	$\frac{PCC - \frac{(TP+FP)(TP+FN)+(FN+TN)(FP+TN)}{(TN+TP+FP+FN)^2}}{1 - \frac{(TP+FP)(TP+FN)+(FN+TN)(FP+TN)}{(TN+TP+FP+FN)^2}}$
Recall	$\frac{(TP)}{(TP+FN)}$
Specificity	$\frac{(TN)}{(TN+FP)}$
PCC	$\frac{(TP)}{(TP+FP)}$
BA	$\frac{(Recall+Specificity)}{2}$
FS	$\frac{2 \times TP}{(2 \times TP + FP + FN)}$
FA	$\frac{(FP)}{(TN+FP)}$
MD	$\frac{(FN)}{(TP+FN)}$

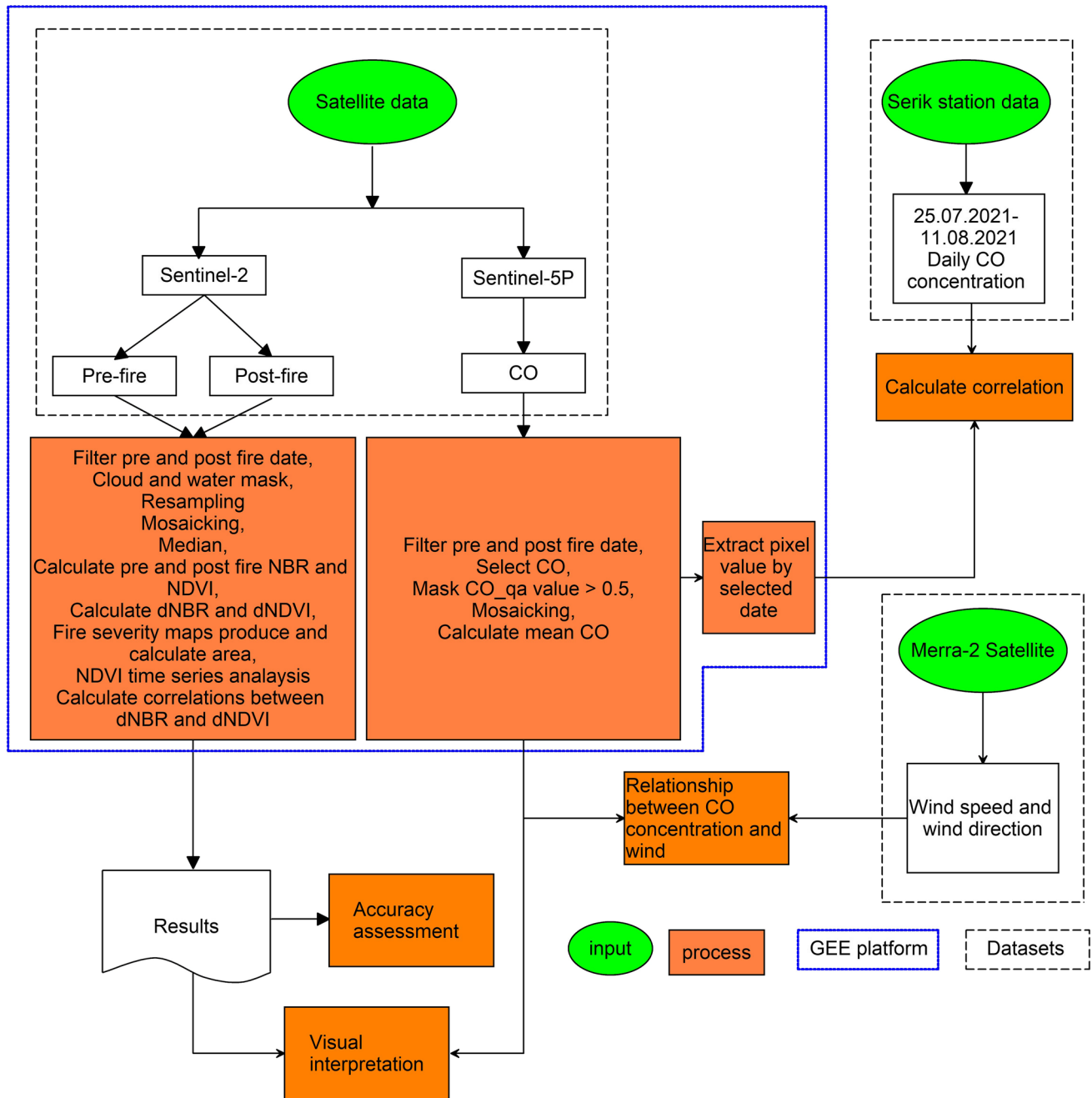


Fig. 2 Workflow chart showing the production of dNBR and dNDVI maps and calculation of CO column number density on the GEE platform

Table 6 Accuracy assessment of burn severity maps obtained according to the dNBR

Region	OA (%)	$\kappa$	Recall (%)	Specificity (%)	PCC (%)	BA (%)	FS (%)	FA (%)	MD (%)	Number of points
Manavgat	81.98	0.636	99.78	63.15	87.01	81.01	93.05	37.99	0.00	1,043
Gundogmus	80.00	0.604	100.00	60.94	70.93	80.47	82.99	39.06	0.00	249
Marmaris	89.28	0.701	100.00	62.01	87.01	81.01	93.05	37.99	0.00	1,738
Bodrum	89.07	0.716	100.00	64.52	86.35	82.26	92.68	35.48	0.00	501
Koycegiz	93.30	0.774	97.98	74.32	93.93	86.15	95.91	25.68	2.02	927

**Table 7** Accuracy assessment of burn severity maps obtained according to the dNDVI

Region	OA (%)	$\kappa$	Recall (%)	Specificity (%)	PCC (%)	BA (%)	FS (%)	FA (%)	MD (%)	Number of points
Manavgat	85.06	0.638	99.34	58.61	81.64	78.97	89.62	41.39	0.66	1,043
Gundogmus	74.79	0.498	98.31	51.67	66.67	74.99	79.45	48.33	1.69	249
Marmaris	93.66	0.832	100.00	77.49	91.90	88.75	95.78	22.51	0.00	1,738
Bodrum	88.84	0.709	99.71	64.29	86.32	82.00	92.53	35.71	0.29	501
Koycegiz	94.29	0.824	95.76	88.33	97.09	92.05	96.42	11.67	4.24	927

was 57,828.38 ha. In this determined area, 7,367.79 ha area was not affected by the fire, while 50,460.59 ha area was affected by the fire with different burn severity. The moderate-low severity area in the burned area was calculated as 16,130.90 ha, covering 27.89% of the burned area. The sum of high, moderate-high, and low severity areas is 34,329.69 ha and covers 59.36% of the total area. In the Gundogmus district of Antalya, the entire area affected by the fire is 15,372.07 ha. A place of 2,165.06 ha within the boundaries of the fire area was not affected by the fire at all. This area has a proportion of 14.08% of the entire area. The area affected by the low-severity fire is 5,767.73 hectares. The sum of high, moderate-high, and moderate-low severity areas was calculated as 7,439.28 ha, covering 48.39% of the total area. The entire area was calculated as 10,583.96 ha in the fire that broke out in the Marmaris district of Mugla. Within this area, an 813.18 ha area was determined as unburned. This area corresponds to 7.68% of the entire area. The moderate-high severity area of the region was calculated as 2,889.83 ha. This area has 27.30% of the whole area. High, moderate-low, and low severity areas cover 22,024.79 ha, 2,795.41 ha, and 2,060.75 ha, with a total burned area rate of 19.13%, 26.41%, and 19.47%. The whole area covered by the burned area in the Bodrum district of Mugla is 17,614.88 ha. The unburned area in this area is 2,193.10 ha. This area covers 12.45% of the entire area. The area of moderate-high severity burning in the region is 5,436.63 ha. This area covers 30.86% of the whole area and is the region with the highest burn severity rate. The sum of high, moderate-low, and low severity areas is 9,985.15 ha and covers 56.69% of the total area. Finally, the entire area affected by the fire in the Koycegiz district of Mugla province is 11,363.41 ha. The unburned area covers 2,110.01 ha, 18.57% of the total burned area. The low severity area covers 35.43% of the area, with 4,025.92 ha. The sum of the high, moderate-high, and moderate-low severity areas is 5,227.48 ha and covers 46.00% of the total area. The fire affected a total of 112,762.70 ha area in the Antalya and Mugla provinces. Among the burned areas, the district most affected by the fire was Manavgat, with 57,828.38 ha. The least affected district was Marmaris, with 10,583.96 ha. In the burn severity maps produced, the high severity in all regions was 13.00%, moderate-high severity 22.00%,

moderate low severity 27.00%, low severity 26.00%, and unburned area 13.00%. In the dNDVI, the burning severity was examined at six degrees. In the Manavgat district, while the ratio of high-severity and moderate severity grades in the dNBR was 34.64%, the sum of very high severity and high severity grades in the dNDVI was calculated as 41.17%. In the forest fire in the basement, while the sum of the ratio of high-severity and moderate severity degrees in the dNBR was 51.50%, the sum of the very high severity and high severity degrees in the dNDVI was calculated as 42.35%. In these two forest fires, it was observed that the areas with high burning degrees were close to each other in both indexes. It was observed that this difference was higher in Gundogmus, Marmaris, and Koycegiz fires.

The correlation between the dNBR and the dNDVI was calculated separately for each fire zone. This calculation was performed using ArcGIS Pro software with 1,000 random points for each fire zone. The dNBR and dNDVI values for each point were then calculated using Microsoft Excel software, Pearson's correlation coefficient  $R$  and  $R^2$  values were calculated, and scatter plot charts were shown (Fig. 4). According to Fig. 4, the highest correlation between the two indexes was observed in the Marmaris fire with the highest  $R$ -value of 0.941 and in the Bodrum fire with an  $R$ -value of 0.915. The lowest  $R$ -value was calculated in the Gundogmus fire at 0.754. It can be easily said that there is a high positive correlation with a correlation value above 0.70 in all fires.

### Determination of green area loss with NDVI and time series analysis

A great deal of forest and vegetation loss occurred in burned areas. It is possible to determine the vegetation density in remotely sensed images with the NDVI (Gitelson et al. 2014; Duarte et al. 2018). It is crucial to reveal a significant difference in the images obtained pre- and post-fire in terms of post-fire destruction. Pre- and post-fire NDVI maps of all burned regions are shown in Fig. 5a-j. When the vegetation density pre-fire is represented by a green colour (pixel value  $\sim 0.9$ ) on the maps, this colour changes to yellow and brown (pixel value  $< 0.1$ ) post-fire.

In most of the studies in the literature, the NDVI is widely used to determine the damage to the plant density of burned

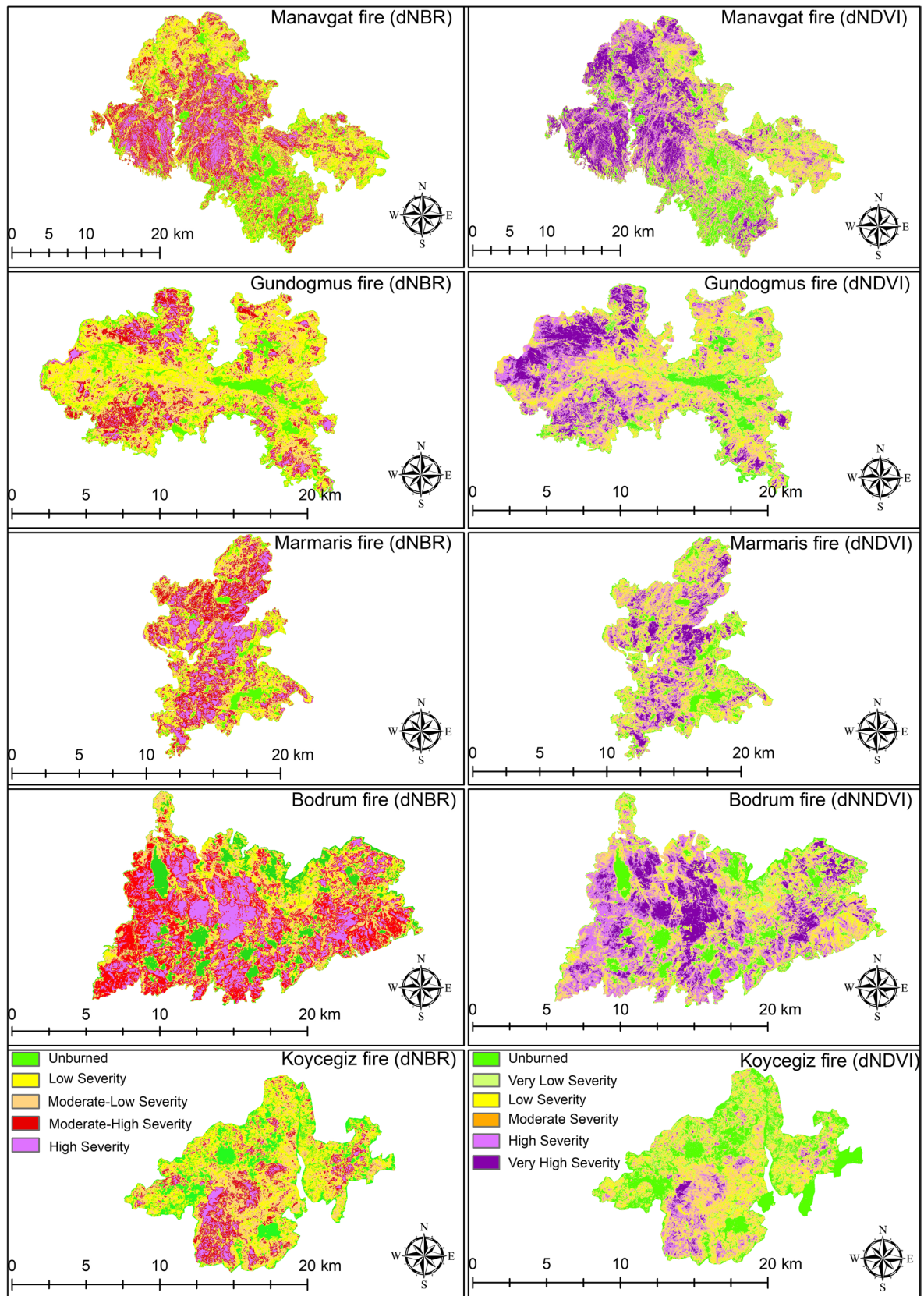


**Fig. 3** Spatial distribution of burn severity maps created according to dNBR and DNDVI indexes

areas (Barbosa et al. 1999; Junaidi et al. 2021; Konkathi and Shetty 2021). Time-series analyses were performed on the GEE platform for the fires in Antalya and Mugla provinces between 01.01.2017 and post-fire until 21.09.2022 (Fig. 6). When Fig. 6 is examined, NDVI values in all fire regions between 2017–2021 were 0.5–0.8 before and remained between 0.2–0.4 after the fire. In 2021–2022, NDVI values fell between 0.1–0.2, sharply decreasing after January. After the cleaning works were carried out in the burned areas after the fire, the effects of the fire became clearer. According to the average NDVI values in burnt areas, it can be said that shrubs and bare land remain.

### Spatio-temporal distribution of CO column number density over post fires

After the forest fires in Antalya and Mugla in 2021, plenty of CO gas was emitted into the atmosphere, especially from the trees that were not completely burned. To better observe the amount of this emitted gas and its increase during the fire, CO gas time series were created for each fire zone between 01.01.2021 and 31.12.2021 (Fig. 7). The time series created for each fire zone represents the average value of the pixels within the fire boundaries. According to Fig. 7, while the average CO value was around 0.03 mol/m<sup>2</sup> over the past one-year period, it reached 0.14 mol/m<sup>2</sup> levels during the fires (red box). After the fires, the CO remained at an average of 0.05 mol/m<sup>2</sup> until August (blue box). The decrease to 0.03 mol/m<sup>2</sup> level was realised after September. According to these results, CO gas decreased to the average level one month after the fire.

Pollutant gases emitted by burning fires to the atmosphere tend to spread due to various atmospheric conditions, especially wind. Especially the fact that the fires that occurred in the Mediterranean region in 2021 were close to each other, both spatially and temporally, caused the spread of polluting gases over large areas. For this purpose, the fires in Antalya and Marmaris provinces were investigated in wide acreages. The amounts of CO emitted into the atmosphere during the Antalya and Mugla forest fires in the summer of 2021 are shown in Fig. 8a–d. These three categories were used in the legend to represent the CO amount. Date ranges were determined as pre-fire, during the fire, and post-fire. The maps covering the entire region were filtered on the GEE platform and created an image collection. The desired date range images were obtained by applying the median statistics on the resulting map collections. The fire started in Manavgat between 18–29 July 2021, and the CO column number density in the atmosphere was monitored between 0.022–0.192 mol/m<sup>2</sup> (Fig. 8a). This value showed that the average CO value of 0.03 mol/m<sup>2</sup> started to increase with the effect of the fire. With the addition of the Koycegiz fire to the Manavgat fire that continued between 26 July–06 August

2021, the CO value reached a maximum of 0.333 mol/m<sup>2</sup> (Fig. 8b–c). The CO value decreased to 0.071 mol/m<sup>2</sup> between 02–15 August on the dates that continued with the fire extinguishing study (Fig. 8d).

It has been observed that CO gas is mainly concentrated in the Mediterranean when the fire started, continued, and ended. The effect of the wind was considered in interpreting the CO gas throughout the date range of analyses. Hourly wind speeds and directions from the Merra-2 satellite were obtained separately for each fire zone. In the given geographic information systems environment, a map showing the fire speed and directions was produced by using the kriging interpolation method (Fig. 9). According to the map, it was observed that the prevailing wind direction in all burned areas was from Northeast to Northwest. The average wind speed varies between 2.55 m/s and 7.66 m/s. It was observed that the wind speed increased significantly from South to West (Fig. 9a). The high-resolution Worldview satellite image (Fig. 9b) taken at a particular time of the fire confirms the map produced. It was observed that the gases emitted into the atmosphere from the burning area moved towards the Southwest and concentrated on the sea.

### Calculation of Sentinel-5P CO column number density

The near-surface atmospheric CO concentration values were measured at the Serik station closest to the fire area. The daily averages of the station data pre- and post-fire are shown in Fig. 10. On average, CO concentration values were around 200 µg/m<sup>3</sup> between July 25 and August 4, 2021. It reached a maximum above 600 µg/m<sup>3</sup> between August 4 and 6, 2021, and decreased below 200 µg/m<sup>3</sup> between August 8 and 11, 2021. The TROPOMI values are compatible with the maps in Figs. 7 and 8. The increases in the CO concentration value in Fig. 8b and c are also consistent with the value between August 4 and 6, 2021, at the measuring station. Unfortunately, there is no data at the station between August 3 and 7, 2021.

The correlation (R-value) between TROPOMI pixel values and Serik station measurements was calculated as 0.705 (Fig. 11), which indicates a high degree of agreement between the two data. This compatibility emphasizes that TROPOMI data is useful for spatio-temporal monitoring of post-fire pollutants such as CO.

When the results in this study were compared with other studies in the literature, it was seen that similar results were obtained. For example, Zheng et al. (2019) compared the NO<sub>2</sub> concentration obtained from TROPOMI with remote sensing methods with ground measurement stations over one year and found R<sup>2</sup> = 0.72. Magro et al. (2021) monitored the CO and CH<sub>4</sub> values of TROPOMI in forest fires in Portugal. They compared

**Table 8** Areas and ratios calculated according to burn severity

Region	Classes	dNBR		dNDVI	
		Area (ha)	Ratio (%)	Area (ha)	Ratio (%)
Manavgat	Very High severity	-	-	11,481.97	19.86
	High Severity	7,209.92	12.47	12,323.54	21.31
	Moderate-High Severity	12,822.24	22.17	-	-
	Moderate severity	-	-	14,579.27	25.21
	Moderate-Low Severity	16,130.90	27.89	-	-
	Low Severity	14,297.53	24.72	6,786.12	11.73
	Very low severity	-	-	4,957.64	8.57
	Unburned	7,367.79	12.74	7,699.85	13.31
	Total	57,828.38		57,828.38	
Gundogmus	Very High severity	-	-	2,051.64	13.35
	High Severity	879.43	5.72	2,584.67	16.81
	Moderate-High Severity	2,282.38	14.85	-	-
	Moderate severity	-	-	4,840.93	31.49
	Moderate-Low Severity	4,277.47	27.83	-	-
	Low Severity	5,767.73	37.52	2,674.06	17.40
	Very low severity	-	-	1,542.21	10.03
	Unburned	2,165.06	14.08	1,678.57	10.92
	Total	15,372.07		15,372.07	
Marmaris	Very High severity	-	-	1,378.56	13.02
	High Severity	2,024.79	19.13	1,850.11	17.48
	Moderate-High Severity	2,889.83	27.30	-	-
	Moderate severity	-	-	3,235.11	30.57
	Moderate-Low Severity	2,795.41	26.41	-	-
	Low Severity	2,060.75	19.47	1,747.21	16.51
	Very low severity	-	-	984.53	9.30
	Unburned	813.18	7.68	1,388.46	13.12
	Total	10,583.96		10,583.96	
Bodrum	Very High severity	-	-	3,008.19	17.08
	High Severity	3,636.71	20.65	4,451.91	25.27
	Moderate-High Severity	5,436.63	30.85	-	-
	Moderate severity	-	-	4,778.26	27.13
	Moderate-Low Severity	3,633.89	20.63	-	-
	Low Severity	2,714.55	15.41	1,881.31	10.68
	Very low severity	-	-	1,325.58	7.53
	Unburned	2,193.10	12.45	2,169.65	12.32
	Total	17,614.88		17,614.88	
Koycegiz	Very High severity	-	-	281.57	2.48
	High Severity	730.87	6.43	900.45	7.92
	Moderate-High Severity	1,414.38	12.45	-	-
	Moderate severity	-	-	2,949.01	25.95
	Moderate-Low Severity	3,082.23	27.12	-	-
	Low Severity	4,025.92	35.43	2,257.64	19.87
	Very low severity	-	-	1,515.15	13.33
	Unburned	2,110.01	18.57	3,459.60	30.45
	Total	11,363.41		11,363.41	

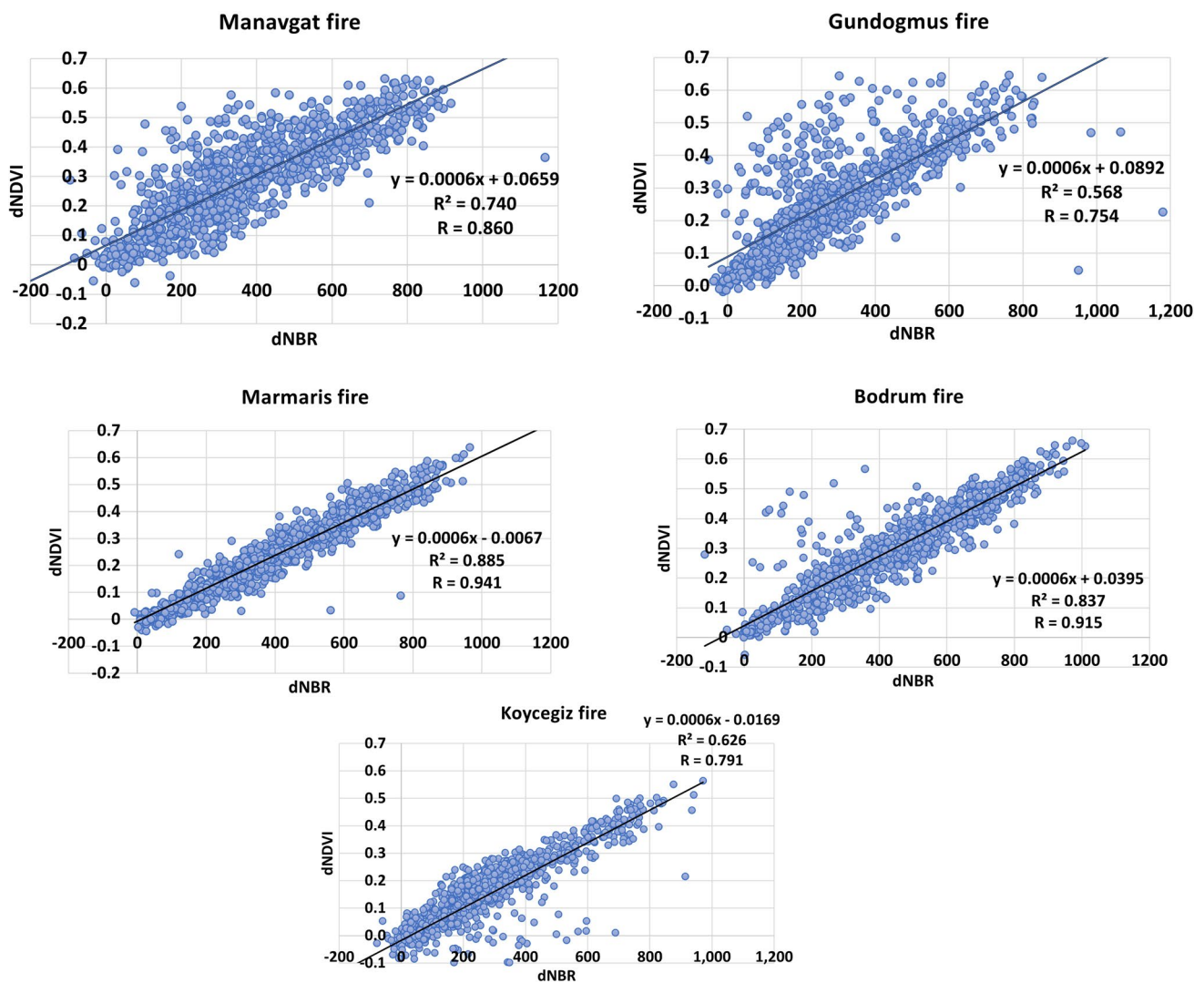


Fig. 4 Correlation analysis for the dNBR and dNDVI

their results with the ground measurement station and observed an  $R = 0.50$  correlation. Ghasempour et al. (2021) conducted research in Türkiye. They investigated the effect of polluting gases in the air during the COVID-19 epidemic period, compared TROPOMI SO<sub>2</sub> and NO gases with the station measurements we used similarly in Türkiye, and obtained correlation coefficients of 0.65 and 0.83, respectively.

## Discussion

### Detection of areas and accuracy analysis with the dNBR and dNDVI

The spatial and temporal resolutions of Sentinel-2 images are better than medium-resolution MODIS, AVHRR, and

Landsat data. These low-resolution images have been used in many studies on forest fires (Escuin et al. 2008; Vanderhoof et al. 2017; Teodoro and Amaral 2019; Youn and Jeong 2019; Cahyono et al. 2021; Chen et al. 2021; Pelletier et al. 2021). Sentinel images enabled the results to have higher spatial resolution and to collect data at more frequent intervals during long fire periods.

The produced maps showed that the area affected by the wildfire was calculated as 112,762.70 ha. The map analysis in this study unearthed that the most affected region by the wildfires was the Manavgat district of Antalya. The total area damaged by the fires in the district was approximately 57,828.38 ha. The area least damaged by the fires was the Marmaris district of Mugla, with 10,583.96 ha. These sensitive calculations are superior knowledge for decision-makers regarding the rehabilitation of burned areas and the sustainability of forest areas.

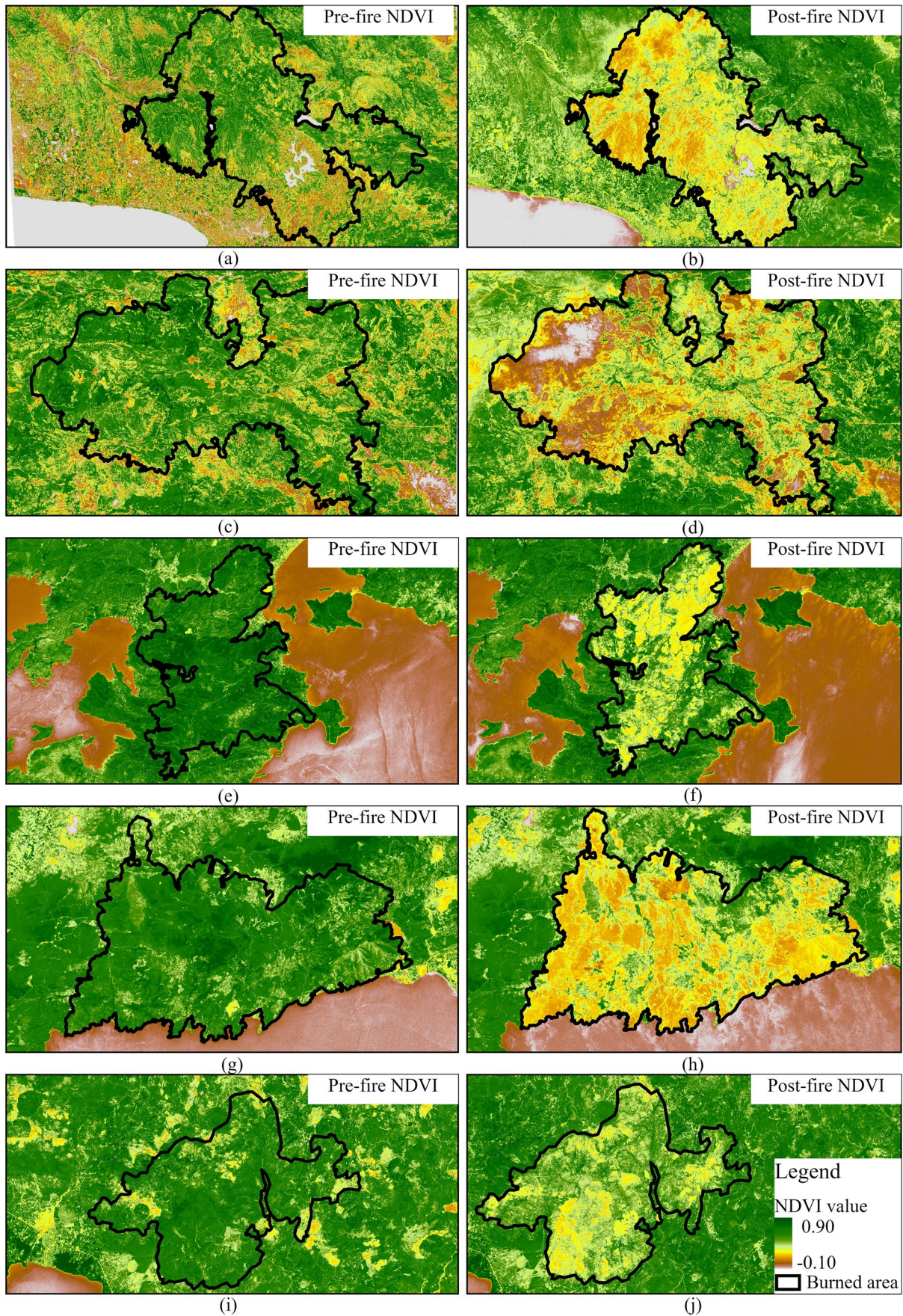


**Fig. 5** NDVI values of all burned regions pre-fire and post-fire: (a) Manavgat pre-fire map, (b) Manavgat post-fire map, (c) Gundogmus pre-fire map, (d) Gundogmus post-fire map, (e) Marmaris pre-fire map, (f) Marmaris post-fire map, (g) Bodrum pre-fire map, (h) Bodrum

In this study, detecting fire areas using the dNBR computed from Sentinel-2 images was very accurate. In previous studies, Botella-Martínez & Fernández-Manso (2017) calculated the dNBR for different fire zones with the OA ranging from 72.1 to 94.8 and  $\kappa$  from 0.61 to 0.92. Llorens et al. (2021) also detected forest fires with the dNBR using Sentinel-2 images. In their study, the classification accuracy was calculated with Kappa statistics, and the  $\kappa$  value ranged from 0.69 to 0.73. Morresi et al. (2022) used the RdNBR and improved the OA and  $\kappa$  values ranging from 76.9% to 83.7% and from 0.61 to 0.72, respectively, in the burn severity maps produced using Sentinel 2 images. Consequently, in our and other researchers' studies, the success of the dNBR used in detecting the burned areas was supported by the statistical tests. Therefore, the results of our study are entirely consistent with the other studies conducted.

### NDVI time series analysis

Detecting the losses in the post-fire vegetation mass with satellite images is an accepted approach discussed in many articles. NDVI time series analysis monitors vegetation changes, especially in areas rehabilitated after wildfires (Cuevas-González et al. 2009; Van Leeuwen et al. 2010; Lanorte et al. 2014; Landi et al. 2021). It is commonly used to detect vegetation density changes

before and after a wildfire. Díaz-Delgado et al. (2003) reported that post-fire NDVI values decreased to 0.36 in areas with high burn severity. Telesca & Lasaponara (2006) examined the dynamic behavior of pre- and post-fire vegetation in a burned forest area through NDVI time series analysis. They found a sharp decrease in post-fire NDVI values in Northern Italy. Lanorte et al. (2014) applied SPOT-VEGETATION NDVI time series analysis. It was determined that the pixel values changes before and after the fire ranged from 0.6 to 0.8 and 0.2 to 0.3, respectively.

Similarly, our study showed that sharp decreases were observed in NDVI values in NDVI time series analysis performed before and after the fire. When previous studies were examined, it was observed that there were sharp decreases in NDVI values after the fire. In this respect, NDVI is very important for monitoring vegetation losses. In this study, the areas where the fire occurred are dominated by maquis and red pine vegetation. After the fire, NDVI values were between 0.2–0.4. This result showed us that there was a significant decrease in the dense vegetation after the fire. It was observed that NDVI values decreased to 0.1–0.2 levels after the cleaning works carried out by the Regional Directorate of Forestry teams, especially within a year after the fire. When these values are considered, it has been observed that bare land and very little vegetation remained in the region after the fire.

It was understood that some burnt trees and sparse vegetation remained after the fire in the burned areas where maquis and red pine vegetation dominate. Therefore, the follow-up of rehabilitation studies to be carried out with annual NDVI follow-ups in the following years will reveal the speed and amount of recovery.

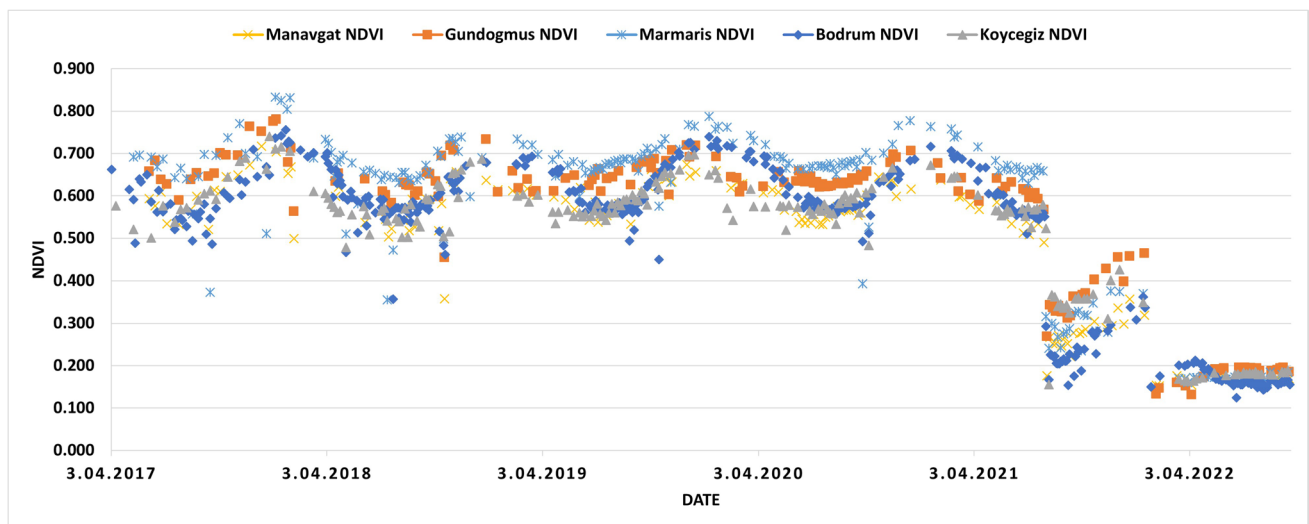


**Fig. 6** NDVI time series analysis

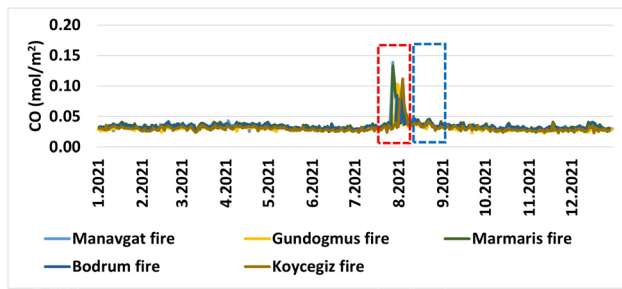
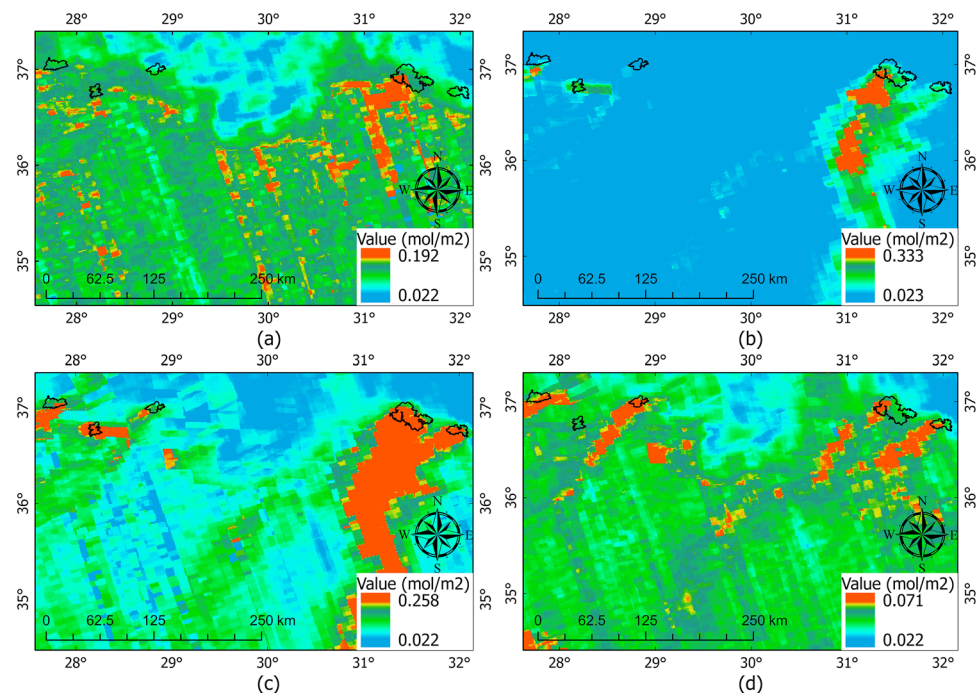


**Fig. 7** CO column number density time series chart for each fire area

## CO column number density

In this study, the amount of CO gas released into the atmosphere in forest fires was determined by the TROPOMI device. It was observed that the average CO content increased from  $0.03 \text{ mol/m}^2$  to  $0.15 \text{ mol/m}^2$  in all fire zones and then decreased to  $0.03 \text{ mol/m}^2$  levels in one month after the fire. On the other hand, if the study carried out in the vast region covering the entire fire zones, the CO gas gathering together in the atmosphere by the affect of wind and reached a maximum level of  $0.333 \text{ mol/m}^2$  with an increase of 1,010% in the wildfire areas. The World Health Organization (WHO) has declared the upper limit of CO  $11,440 \mu\text{g/m}^3$  in 8 h. The amount of CO emitted into the atmosphere after the fire was measured as approximately  $680 \mu\text{g/m}^3$  from the Serik station, which is 34 km from the closest ground stations to the fire areas. This value is likely to approach the upper limits reported by WHO in the atmosphere over

**Fig. 8** CO column number density covers all regions pre and post-fire; the date ranges represent the CO column number density map: (a) 18.07.2021–29.07.2021, (b) 26.07.2021–04.08.2021, (c) 29.07.2021–06.08.2021, (d) 02.08.2021–15.08.2021



the fire zone. This level will cause adverse health effects on living things. For example, outdoor CO levels are a risk for lung and heart patients, such as COPD, asthma, and cardiovascular diseases (Fu et al. 2020).

Fires are natural disasters that occur for various reasons. These natural disasters frequently occur, especially in Mediterranean countries where the hot climate is in question. Although it is seen in this study that harmful gases such as CO gas spread to the seas, other forest fires that may occur in the future may affect the settlements with the effect of the wind. From this point of view, this study is vital regarding air pollution and precautions that may be effective after fires.

## Conclusion

In 2021, forest fires in the Mediterranean and Aegean regions, especially in Mugla and Antalya, caused great environmental and ecological disasters. RS techniques were used to reveal the forest fires' severity and the effect of fires on the region's flora and fauna. In this study, Sentinel-2 (MSI) satellite data were used for calculating dNBR and dNDVI spectral indices to determine the severity of the fire. Besides Sentinel 5P data were used for monitoring pollutant gasses after the fire. In the regions where the fire occurred, burn severity degrees were determined separately for the dNBR and dNDVI indexes, and fire severity was graded in five classes for dNBR and six classes for dNDVI. According to the burn severity maps obtained with the dNBR and dNDVI indexes, the affected areas in

**Fig. 9** Map showing wind speed and direction: a) Represents wind speed and direction in fire areas, b) High resolution satellite image downloaded from NASA’s site during the fire (<https://eoimages.gsfc.nasa.gov/images/imagerecords/148000/148650/fireturkey>)

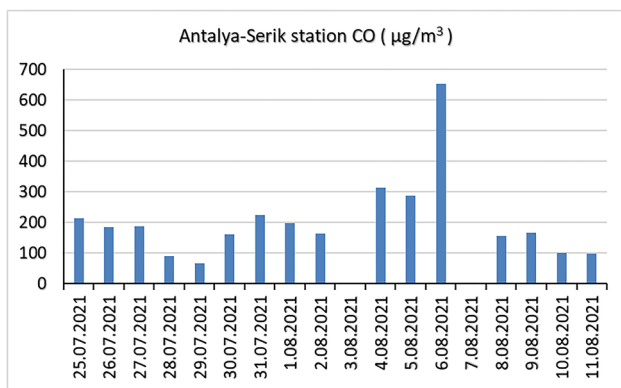
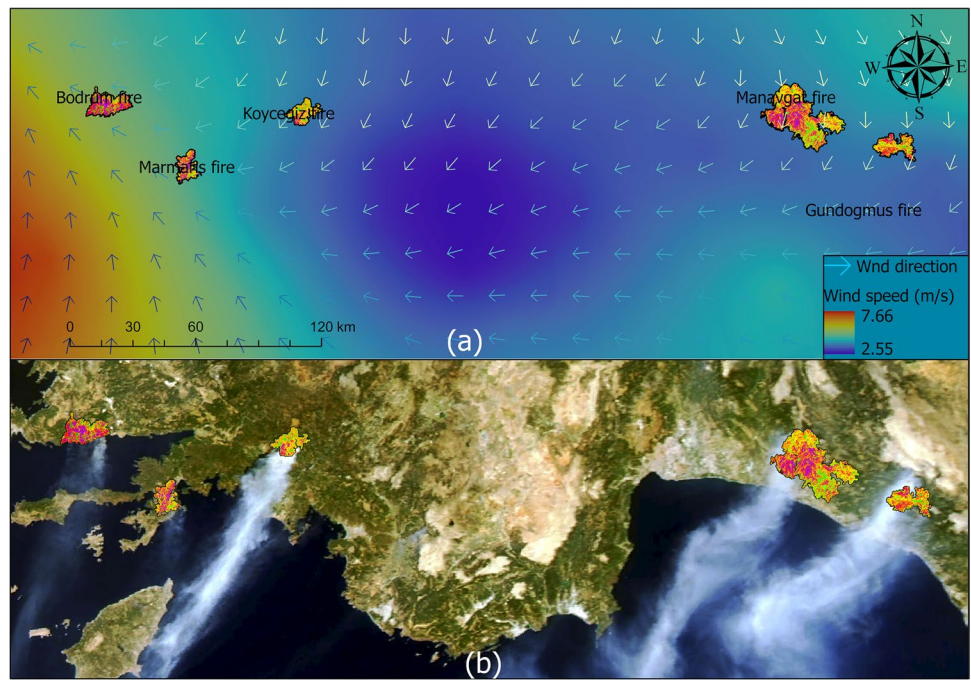
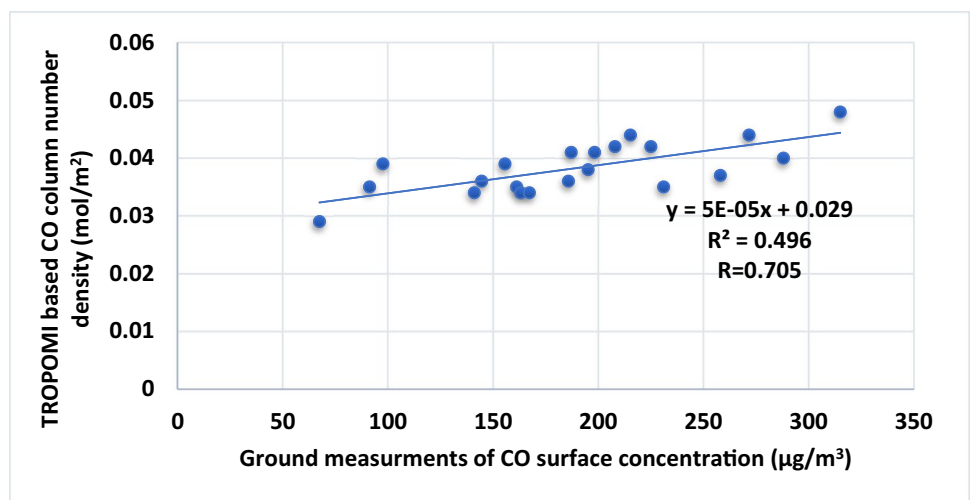


**Fig. 10** Carbon monoxide concentration values measured from Antalya Serik station

**Fig. 11** TROPOMI Serik station measurement values regression analysis



Manavgat, Gundogmus, Marmaris, Bodrum, and Koycegiz districts were calculated as 57,828.38 ha, 15,372.07 ha, 10,583.96 ha, 17,614.88 ha, and 11,363.41 ha, respectively. According to the burn severity maps obtained with dNBR, the sum of the areas of high severity and moderate severity constitutes 34.64%, 20.57%, 46.43%, 51.50%, and 18.88% of the entire region, respectively. Likewise, according to the burn severity maps obtained with dNDVI, the sum of the areas of very high severity and high severity constitutes 41.17%, 30.16%, 30.50%, 42.35%, and 10.40% of the entire region, respectively. The dNBR and dNDVI indexes have been demonstrated again in this study, thanks to Sentinel-2 satellite images, that they are very effective in producing burn severity maps by taking into account the situations pre

and post-fire. At the same time, with the NDVI time series analyses calculated from 2017 to the end of 2022, serious information was obtained about the change in plant density before and after the fire. It has been observed that the forest areas in the region have turned into bare land, with NDVI values ranging from 0.5 to 0.8 and NDVI values ranging between 0.1–0.2 after the fire in forests generally covered with scrub and red pine. Time series analysis is critical for monitoring plants' phenological cycle and vegetation recovery. In addition to field studies and monitoring, RS techniques provide significant advantages, especially for large areas and hard-to-reach lands.

After fires, various harmful gases such as CO, CO<sub>2</sub>, and CH<sub>4</sub> are emitted in abundance into the atmosphere. A one-year investigation was made with Sentinel-5P satellite data in each fire zone, and the CO level increased from 0.03 mol/m<sup>2</sup> on average to 0.14 mol/m<sup>2</sup> during the fire. The CO gas from the forest fires that broke out at about the same time spread over large areas with the effect of the wind. Although the gases spread over large areas, they reached 0.333 mol/m<sup>2</sup> levels with the accumulation of CO gases emitted from all fire areas. Mediterranean forest fires in 2021 concentrated on the Mediterranean with the effect of the wind. Although CO gas accumulated mainly above the Mediterranean, it has also affected many regional settlements. The increase in CO in the atmosphere during fires adversely affects the life of all breathing creatures until they decrease to normal levels. It was noteworthy that the CO gas level remained at 0.05 mol/m<sup>2</sup> for approximately one month, especially after the fire, which is a significant result for this study. Considering this result, it poses a risk, especially for chronic lung and cardiovascular patients in areas close to settlements. CO gas, which continues to exist in the atmosphere for a long time, such as a month, will adversely affect humans and other breathing creatures, such as birds. Therefore, monitoring these gases with RS techniques is vital for managers and decision-makers to draw up emergency action plans when their emissions need to be monitored.

Burn severity maps were produced in this study, and burned areas were graded according to dNBR and dNDVI indexes. It has been revealed that the burning area size and severity also affect the gas concentration to be released. Therefore, in natural disasters such as fire, besides determining the severity of the fire, it is also essential to investigate the environmental effects, especially in terms of air pollution. Many countries have local ground monitoring stations to monitor and detect harmful gases in the air. However, satellite systems enable monitoring these gases globally at almost zero cost. This study revealed that the gases that cause environmental pollution and global warming after the fire could be quickly monitored with satellite images.

This study shows that the integrated use of Sentinel-2 and Sentinel-5P data will be significant in monitoring forest fires

and revealing both the atmospheric and ecological effects of wildfire. In addition, all image processing tasks were performed on the GEE platform in the study. In addition, it has been shown that this platform is suitable for fast, reliable, and cost-effective damage assessment and environmental impact monitoring in wildfires occurring in different parts of the world.

**Authors' contribution** Osman Salih YILMAZ: conceptualisation, data collection, analysing, and writing; Ugur ACAR: literature search and review, analysing, visualisation, Fusun BALIK SANLI, Fatih GULGEN, and Ali Murat ATES: conceptualisation, writing, validation, review, and editing.

**Data availability** All data used in the current study are available free of charge to all users on the GEE platform and can be obtained here. Otherwise, it can be available from the corresponding author upon reasonable request.

## Declarations

**Ethical Approval** All authors in this article have read, understood, and prepared under the "Authors' Ethical Responsibilities" in the Authors' Submission guidelines.

**Competing interests** The authors declare no competing interests.

## References

- Arekhi M, Goksel C, Balik Sanli F, Senel G (2019) Comparative Evaluation of the Spectral and Spatial Consistency of Sentinel-2 and Landsat-8 OLI Data for Igneada Longos Forest. *ISPRS Int J Geo-Information* 8:56. <https://doi.org/10.3390/ijgi8020056>
- Astola H, Häme T, Sirro L et al (2019) Comparison of Sentinel-2 and Landsat 8 imagery for forest variable prediction in boreal region. *Remote Sens Environ* 223:257–273. <https://doi.org/10.1016/j.rse.2019.01.019>
- Atun R, Kalkan K, Gürsoy Ö (2020) Determining The Forest Fire Risk with Sentinel 2 Images. *Turkish J Geosci* 1:22–26
- Bar S, Parida BR, Pandey AC (2020) Landsat-8 and Sentinel-2 based Forest fire burn area mapping using machine learning algorithms on GEE cloud platform over Uttarakhand, Western Himalaya. *Remote Sens Appl Soc Environ* 18:100324. <https://doi.org/10.1016/j.rsase.2020.100324>
- Barbosa PM, Grégoire JM, Pereira JMC (1999) An algorithm for extracting burned areas from time series of AVHRR GAC data applied at a continental scale. *Remote Sens Environ* 69:253–263. [https://doi.org/10.1016/S0034-4257\(99\)00026-7](https://doi.org/10.1016/S0034-4257(99)00026-7)
- Boer MM, Macfarlane C, Norris J et al (2008) Mapping burned areas and burn severity patterns in SW Australian eucalypt forest using remotely-sensed changes in leaf area index. *Remote Sens Environ* 112:4358–4369. <https://doi.org/10.1016/j.rse.2008.08.005>
- Botella-Martínez MA, Fernández-Manso A (2017) Estudio de la severidad post-incendio en la comunidad Valenciana comparando los índices dNBR, RdNBR y RBR a partir de imágenes landsat 8. *Rev Teledetec* 2017:33–47. <https://doi.org/10.4995/raet.2017.7095>
- Cahyono BE, Fibyana V, Nugroho AT, Subekti A (2021) Mapping and analysis burned area based on LANDSAT 8 OLI/TIRS and hotspots data in palangkaraya of central kalimantan province - Indonesia. *J Phys Conf Ser* 1825:. <https://doi.org/10.1088/1742-6596/1825/1/012087>

- Chen D, Fu C, Hall JV et al (2021) Spatio-temporal patterns of optimal Landsat data for burn severity index calculations: Implications for high northern latitudes wildfire research. *Remote Sens Environ* 258:112393. <https://doi.org/10.1016/j.rse.2021.112393>
- Cheret V, Denux J-P (2011) Analysis of MODIS NDVI time series to calculate indicators of Mediterranean forest fire susceptibility. *Giscience Remote Sens* 48:171–194
- Chung M, Kim Y (2021) Wildfire-induced Change Detection Using Post-fire VHR Satellite Images and GIS Data. *Korean J Remote Sens* 37:1389–1403. <https://doi.org/10.7780/kjrs.2021.37.5.3.5>
- Cordeiro MCR, Martínez JM, Peña-Luque S (2021) Automatic water detection from multidimensional hierarchical clustering for Sentinel-2 images and a comparison with Level 2A processors. *Remote Sens Environ* 253: <https://doi.org/10.1016/j.rse.2020.112209>
- Cuevas-González M, Gerard F, Balzter H, Riaño D (2009) Analysing forest recovery after wildfire disturbance in boreal Siberia using remotely sensed vegetation indices. *Glob Chang Biol* 15:561–577. <https://doi.org/10.1111/j.1365-2486.2008.01784.x>
- De la Rosa JM, González-Pérez JA, González-Vázquez R et al (2008) Use of pyrolysis/GC–MS combined with thermal analysis to monitor C and N changes in soil organic matter from a Mediterranean fire affected forest. *CATENA* 74:296–303
- Delcourt CJF, Combee A, Izbicki B et al (2021) Evaluating the differenced normalized burn ratio for assessing fire severity using sentinel-2 imagery in northeast siberian larch forests. *Remote Sens* 13:1–20. <https://doi.org/10.3390/rs13122311>
- Díaz-Delgado R, Lloret F, Pons X (2003) Influence of fire severity on plant regeneration by means of remote sensing imagery. *Int J Remote Sens* 24:1751–1763. <https://doi.org/10.1080/0143160210144732>
- Dindaroglu T, Babur E, Yakupoglu T, et al (2021) Evaluation of geomorphometric characteristics and soil properties after a wildfire using Sentinel-2 MSI imagery for future fire-safe forest. *Fire Saf J* 122: <https://doi.org/10.1016/j.firesaf.2021.103318>
- Dixon DJ, Callow JN, Duncan JMA et al (2022) Regional-scale fire severity mapping of Eucalyptus forests with the Landsat archive. *Remote Sens Environ* 270:112863. <https://doi.org/10.1016/j.rse.2021.112863>
- Duarte L, Teodoro AC, Monteiro AT et al (2018) QPhenoMetrics: An open source software application to assess vegetation phenology metrics. *Comput Electron Agric* 148:82–94
- Efthimiou N, Psomiadis E, Panagos P (2020) Fire severity and soil erosion susceptibility mapping using multi-temporal Earth Observation data: The case of Mati fatal wildfire in Eastern Attica Greece. *Catena* 187:104320. <https://doi.org/10.1016/j.catena.2019.104320>
- Escuin S, Navarro R, Fernández P (2008) Fire severity assessment by using NBR (Normalized Burn Ratio) and NDVI (Normalized Difference Vegetation Index) derived from LANDSAT TM/ETM images. *Int J Remote Sens* 29:1053–1073. <https://doi.org/10.1080/01431160701281072>
- Esemen K, (2011) Forest Fires analysis using satellite imagery. Master's Thesis, Istanbul Technical Univesity, Istanbul, Türkiye
- Eva H, Lambin EF (2000) Fires and land-cover change in the tropics: a remote sensing analysis at the landscape scale. *J Biogeogr* 27:765–776
- Faisal M, Prakoso KA, Sanjaya H et al (2021) Spatio-temporal analysis of air pollutants changes during the COVID-19 using sentinel-5P in google earth engine (Case Study: Java Island). *IEEE Asia-Pacific Conference on Geoscience, Electronics, and Remote Sensing Technology (AGERS)* 102–108. <https://doi.org/10.1080/19475705.2021.1920477>
- Fu F, Purvis-Roberts KL, Williams B (2020) Impact of the covid-19 pandemic lockdown on air pollution in 20 major cities around the world. *Atmosphere (Basel)* 11: <https://doi.org/10.3390/atmos11111189>
- García-Llamas P, Suárez-Seoane S, Fernández-Guisuraga JM et al (2019) Evaluation and comparison of Landsat 8, Sentinel-2 and Deimos-1 remote sensing indices for assessing burn severity in Mediterranean fire-prone ecosystems. *Int J Appl Earth Obs Geoinf* 80:137–144. <https://doi.org/10.1016/j.jag.2019.04.006>
- Ghasempour F, Sekertekin A, Kutoglu SH (2021) Google Earth Engine based spatio-temporal analysis of air pollutants before and during the first wave COVID-19 outbreak over Turkey via remote sensing. *J Clean Prod* 319:128599. <https://doi.org/10.1016/j.jclepro.2021.128599>
- Gibson R, Danaher T, Hehir W, Collins L (2020) A remote sensing approach to mapping fire severity in south-eastern Australia using sentinel 2 and random forest. *Remote Sens Environ* 240:111702. <https://doi.org/10.1016/j.rse.2020.111702>
- Giddey BL, Baard JA, Kraaij T (2022) Verification of the differenced Normalised Burn Ratio (dNBR) as an index of fire severity in Afrotropicate Forest. *South African J Bot* 146:348–353. <https://doi.org/10.1016/j.sajb.2021.11.005>
- Gitelson AA, Peng Y, Huemmrich KF (2014) Relationship between fraction of radiation absorbed by photosynthesizing maize and soybean canopies and NDVI from remotely sensed data taken at close range and from MODIS 250 m resolution data. *Remote Sens Environ* 147:108–120
- Goodwin NR, Collett LJ (2014) Development of an automated method for mapping fire history captured in Landsat TM and ETM+ time series across Queensland, Australia. *Remote Sens Environ* 148:206–221. <https://doi.org/10.1016/j.rse.2014.03.021>
- Hantson S, Padilla M, Corti D, Chuvieco E (2013) Strengths and weaknesses of MODIS hotspots to characterize global fire occurrence. *Remote Sens Environ* 131:152–159. <https://doi.org/10.1016/j.rse.2012.12.004>
- Hope A, Tague C, Clark R (2007) Characterizing post-fire vegetation recovery of California chaparral using TM/ETM+ time-series data. *Int J Remote Sens* 28:1339–1354. <https://doi.org/10.1080/01431160600908924>
- Hu X, Ban Y, Nascetti A (2021) Uni-temporal multispectral imagery for burned area mapping with deep learning. *Remote Sens* 13: <https://doi.org/10.3390/rs13081509>
- Junaidi SN, Khalid N, Othman AN, et al (2021) Analysis of the Relationship between Forest Fire and Land Surface Temperature using Landsat 8 OLI/TIRS Imagery. *IOP Conf Ser Earth Environ Sci* 767: <https://doi.org/10.1088/1755-1315/767/1/012005>
- Keeley JE (2008) Fire: encyclopedia of ecology. In: Jørgensen SE, Fath BD (eds). Academic Press, Cambridge, MA, p 1557–1564
- Key CH, Benson NC (2006) Landscape assessment: sampling and analysis methods. USDA Forest service, rocky mountain research station general technical report RMRS-GTR-164-CD, Ogden
- Konkathi P, Shetty A (2021) Inter comparison of post-fire burn severity indices of Landsat-8 and Sentinel-2 imagery using Google Earth Engine. *Earth Sci Informatics* 14:645–653. <https://doi.org/10.1007/s12145-020-00566-2>
- Kulakowski D, Veblen TT (2007) Effect of prior disturbances on the extent and severity of wildfire in Colorado subalpine forests. *Ecology* 88:759–769
- Landi MA, Di Bella CM, Bravo SJ, Bellis LM (2021) Structural resistance and functional resilience of the Chaco forest to wild-land fires: an approach with MODIS time series. *Austral Ecol* 46:277–289. <https://doi.org/10.1111/aec.12977>
- Lanorte A, Lasaponara R, Lovallo M, Telesca L (2014) Fisher-Shannon information plane analysis of SPOT/VEGETATION normalized difference vegetation index (NDVI) time series to characterize vegetation recovery after fire disturbance. *Int J Appl Earth Obs Geoinf* 26:441–446. <https://doi.org/10.1016/j.jag.2013.05.008>
- Lentile LB, Holden ZA, Smith AMS et al (2006) Remote sensing techniques to assess active fire characteristics and post-fire effects. *Int J Wildl Fire* 15:319–345. <https://doi.org/10.1071/WF05097>
- Li X, Liu L, Qi S (2018) Forest fire hazard during 2000–2016 in Zhejiang province of the typical subtropical region, China. *Nat Hazards* 94:975–977

- Llorens R, Sobrino JA, Fernández C et al (2021) A methodology to estimate forest fires burned areas and burn severity degrees using Sentinel-2 data Application to the October 2017 fires in the Iberian Peninsula. *Int J Appl Earth Obs Geoinf* 95:102243. <https://doi.org/10.1016/j.jag.2020.102243>
- Magro C, Nunes L, Gonçalves O et al (2021) Atmospheric Trends of CO and CH<sub>4</sub> from Extreme Wildfires in Portugal Using Sentinel-5P TROPOMI Level-2 Data. *Fire* 4:25. <https://doi.org/10.3390/fire4020025>
- Masinda MM, Li F, Qi L et al (2022) Forest fire risk estimation in a typical temperate forest in Northeastern China using the Canadian forest fire weather index: case study in autumn 2019 and 2020. *Nat Hazards* 111:1085–1101
- Mathews LEH, Kinoshita AM (2021) Urban fire severity and vegetation dynamics in southern California. *Remote Sens* 13:1–18. <https://doi.org/10.3390/rs13010019>
- Mehmood K, Bao Y, Petropoulos GP, Abbas R, Abrar MM, Saifullah Mustafa A, Soban A, Saud S, Ahmad M, Hussain I, Fahad S (2021) Investigating connections between COVID-19 pandemic, air pollution and community interventions for Pakistan employing geoinformation technologies. *Chemosphere* 272:129809. <https://doi.org/10.1016/j.chemosphere.2021.129809>
- Michel C, Lioussé C, Grégoire JM et al (2005) Biomass burning emission inventory from burnt area data given by the SPOTVEGETATION system in the frame of TRACE-P and ACE-Asia campaigns. *J Geophys Res Atmos* 110(D9). <https://doi.org/10.1029/2004JD005461>
- Morante-Carballo F, Bravo-Montero L, Carrión-Mero P et al (2022) Forest Fire Assessment Using Remote Sensing to Support the Development of an Action Plan Proposal in Ecuador. *Remote Sens* 14:1–26. <https://doi.org/10.3390/rs14081783>
- Morresi D, Marzano R, Lingua E et al (2022) Mapping burn severity in the western Italian Alps through phenologically coherent reflectance composites derived from Sentinel-2 imagery. *Remote Sens Environ* 269:112800. <https://doi.org/10.1016/j.rse.2021.112800>
- Parks SA, Dillon GK, Miller C (2014) A new metric for quantifying burn severity: The relativized burn ratio. *Remote Sens* 6:1827–1844. <https://doi.org/10.3390/rs6031827>
- Pelletier F, Eskelson BNI, Monleon VJ, Tseng YC (2021) Using landsat imagery to assess burn severity of national forest inventory plots. *Remote Sens* 13:1–20. <https://doi.org/10.3390/rs13101935>
- Picotte JJ, Cansler CA, Kolden CA et al (2021) Determination of burn severity models ranging from regional to national scales for the conterminous United States. *Remote Sens Environ* 263:112569. <https://doi.org/10.1016/j.rse.2021.112569>
- Quintano C, Fernández-Manso A, Stein A, Bijker W (2011) Estimation of area burned by forest fires in Mediterranean countries: A remote sensing data mining perspective. *For Ecol Manage* 262:1597–1607. <https://doi.org/10.1016/j.foreco.2011.07.010>
- Reahard RR, Clark R, Robin C, Zeringue J, McCarty JL (2010) Louisiana air quality-using ASTER, Landsat 5, and MODIS to Assess the impact of sugarcane and marsh burning practices on local air quality. In: AGU fall meeting abstracts. A21B-0051
- Reichle RH, Draper CS, Liu Q et al (2017a) Assessment of MERRA-2 land surface hydrology estimates. *J Clim* 30:2937–2960
- Reichle RH, Liu Q, Koster RD et al (2017b) Land surface precipitation in MERRA-2. *J Clim* 30:1643–1664
- Rouse JW, Haas RH, Schell JA et al (1974) Monitoring the vernal advancement and retrogradation (greenwave effect) of natural vegetation. NASA/GSFC Type III Final Report, Greenbelt, Maryland, p 371
- Satyendra T, Singh RN, Shaishav S (2013) Emissions from crop/biomass residue burning risk to atmospheric quality. *Int Res J Earth Sci* 1:1–5
- Schneising O, Buchwitz M, Reuter M et al (2019) A scientific algorithm to simultaneously retrieve carbon monoxide and methane from TROPOMI onboard Sentinel-5 Precursor. *Atmos Meas Tech* 12:6771–6802. <https://doi.org/10.5194/amt-12-6771-2019>
- Seydi ST, Akhoondzadeh M, Amani M (2021) Wildfire Damage Assessment over Australia Using Sentinel-2 Imagery and MODIS Land Cover Product within the Google Earth Engine Cloud Platform. *Remote Sens* 13:220
- Smith-Ramírez C, Castillo-Mandujano J, Becerra P, et al (2022) Combining remote sensing and field data to assess recovery of the Chilean Mediterranean vegetation after fire: Effect of time elapsed and burn severity. *For Ecol Manage* 503. <https://doi.org/10.1016/j.foreco.2021.119800>
- Storey EA, Lee West KR, Stow DA (2021) Utility and optimization of LANDSAT-derived burned area maps for southern California. *Int J Remote Sens* 42:486–505. <https://doi.org/10.1080/01431161.2020.1809741>
- Telesca L, Lasaponara R (2006) Pre-and post-fire behavioural trends revealed in satellite NDMI time series. *Geophys Res Lett* 33:L14401. <https://doi.org/10.1029/2006GL026630>
- Teodoro A, Amaral A (2019) A Statistical and Spatial Analysis of Portuguese Forest Fires in Summer 2016 Considering Landsat 8 and Sentinel 2A Data. *Environments* 6:36. <https://doi.org/10.3390/environments6030036>
- Tian Y, Sun Y, Borsdorff T et al (2022) Quantifying CO emission rates of industrial point sources from Tropospheric Monitoring Instrument observations. *Environ Res Lett* 17:014057. <https://doi.org/10.1088/1748-9326/ac3b1a>
- Uyeda KA, Stow DA, Riggan PJ (2015) Tracking MODIS NDMI time series to estimate fuel accumulation. *Remote Sens Lett* 6:587–596
- Vahid S, Behrouz S, Yazdani MH, Mohammadkia K (2020) Monitoring, analysis and spatial and temporal zoning of air pollution (carbon monoxide) using Sentinel-5 satellite data for health management in Iran, located in the Middle East. *Air Qual Atmos Health* 13:709–719
- van Gerrevink MJ, Veraverbeke S (2021) Evaluating the hyperspectral sensitivity of the differenced normalized burn ratio for assessing fire severity. *Remote Sens* 13. <https://doi.org/10.3390/rs13224611>
- Van Leeuwen WJD, Casady GM, Neary DG et al (2010) Monitoring post-wildfire vegetation response with remotely sensed time-series data in Spain, USA and Israel. *Int J Wildl Fire* 19:75–93. <https://doi.org/10.1071/WF08078>
- Vanderhoof MK, Fairaux N, Beal YJG, Hawbaker TJ (2017) Validation of the USGS Landsat Burned Area Essential Climate Variable (BAECV) across the conterminous United States. *Remote Sens Environ* 198:393–406. <https://doi.org/10.1016/j.rse.2017.06.025>
- Verhoelst T, Compennolle S, Pinardi G et al (2021) Ground-based validation of the Copernicus Sentinel-5p TROPOMI NO<sub>2</sub> measurements with the NDACC ZSL-DOAS, MAX-DOAS and Pandora global networks. *Atmos Meas Tech* 14:481–510
- Wang Q, Yuan Z, Du Q, Li X (2018) GETNET: A general end-to-end 2-D CNN framework for hyperspectral image change detection. *IEEE Trans Geosci Remote Sens* 57:3–13
- Xulu S, Mbatha N, Peerbhay K (2021) Burned Area Mapping over the Southern Cape Forestry Region, South Africa Using Sentinel Data within GEE Cloud Platform. *ISPRS Int J Geo-Information* 10:511. <https://doi.org/10.3390/ijgi10080511>
- Youn H, Jeong J (2019) Detection of Forest Fire and NBR Mis-classified Pixel Using Multi-temporal Sentinel-2A Images. *Korean J Remote Sens* 35:1107–1115
- Zheng Z, Yang Z, Wu Z, Marinello F (2019) Spatial variation of NO<sub>2</sub> and its impact factors in China: An application of sentinel-5P products. *Remote Sens* 11:1939

**Publisher's note** Springer Nature remains neutral with regard to jurisdictional claims in published maps and institutional affiliations.

Springer Nature or its licensor (e.g. a society or other partner) holds exclusive rights to this article under a publishing agreement with the author(s) or other rightsholder(s); author self-archiving of the accepted manuscript version of this article is solely governed by the terms of such publishing agreement and applicable law.